Nanoscale Res Lett (2010) 5:889–897
DOI 10.1007/s11671-010-9580-7

NANO EXPRESS

# Template-Assisted Synthesis and Characterization of Passivated Nickel Nanoparticles

**E. Veena Gopalan · K. A. Malini · G. Santhoshkumar · T. N. Narayanan · P. A. Joy · I. A. Al-Omari · D. Sakthi Kumar · Yasuhiko Yoshida · M. R. Anantharaman**

Received: 30 December 2009 / Accepted: 15 March 2010 / Published online: 2 April 2010


**Abstract** Potential applications of nickel nanoparticles demand the synthesis of self-protected nickel nanoparticles by different synthesis techniques. A novel and simple technique for the synthesis of self-protected nickel nanoparticles is realized by the inter-matrix synthesis of nickel nanoparticles by cation exchange reduction in two types of resins. Two different polymer templates namely strongly acidic cation exchange resins and weakly acidic cation exchange resins provided with cation exchange sites which can anchor metal cations by the ion exchange process are used. The nickel ions which are held at the cation exchange sites by ion fixation can be subsequently reduced to metal nanoparticles by using sodium borohydride as the reducing agent. The composites are cycled repeating the loading reduction cycle involved in the synthesis procedure. X-Ray Diffraction, Scanning Electron Microscopy, Transmission Electron microscopy, Energy Dispersive Spectrum, and Inductively Coupled Plasma Analysis are effectively utilized to investigate the different structural characteristics of the nanocomposites. The hysteresis loop parameters namely saturation magnetization and coercivity are measured using Vibrating Sample Magnetometer. The thermomagnetization study is also conducted to evaluate the Curie temperature values of the composites. The effect of cycling on the structural and magnetic characteristics of the two composites are dealt in detail. A comparison between the different characteristics of the two nanocomposites is also provided.

**Keywords** Polymer–metal nanocomposites · Strongly acidic cation exchange resin · Weakly acidic cation exchange resin · Nickel nanoparticles · Stuctural and magnetic properties

E. Veena Gopalan · T. N. Narayanan · M. R. Anantharaman (✉)
Department of Physics, Cochin University of Science and Technology, Cochin 682 022, Kerala, India
e-mail: mraiyer@gmail.com

K. A. Malini
Department of Physics, Vimala College, Thrissur 680 009, Kerala, India

G. Santhoshkumar
Department of Physics, Government Arts College, Thiruvananthapuram, Kerala, India

P. A. Joy
Physical Chemistry Division, National Chemical Laboratory, Pune 411 008, India

I. A. Al-Omari
Department of Physics, College of Sciences, Sultan Qaboos University, P O Box 36, PC 123 Muscat, Sultanate of Oman

D. Sakthi Kumar · Y. Yoshida
Bio-Nano Electronics Research Centre, Department of Applied Chemistry, Toyo University, Kawagoe, Saitama 350-8585, Japan

## Introduction

Metal nanoparticles are of great interest because they exhibit interesting optical, electronic, magnetic, and chemical properties. They find potential applications in various optoelectronic devices, as catalysts in chemical reactions and also as biosensors [1–4]. Synthesis of metal nanoparticles either in the form of independent entities or in matrices thus assume significance and are of interest to chemists and physicists alike. Preparation of nanoparticles of Fe/Ni/Co is not very easy and hence novel methods and alternate routes are normally scouted for. The large surface area of unprotected metal nanoparticle is prone to oxidation

and thus conventional methods for the synthesis of metal nanoparticles are not feasible. Self-protected metal particles embedded in host matrices are thus a viable alternative. Stabilization of metal nanoparticles by employing capping agents or coating with surfactants are usually adopted to [5, 6]. The fabrication of polymer-stabilized metal nanoparticles is a promising solution to the metal nanoparticle instability and thus they attract the attention of material scientists and technologists [7, 8]. The areas of practical applications of metal–polymer composite are in spin-polarized devices, sensors [9], and carriers for drug delivery [10] and in catalysis [11].

A wide variety of methods are adopted for the fabrication of metal–polymer composites which include both physical and chemical techniques. Examples of physical methods are cryo chemical deposition of metals on polymeric supports and simultaneous plasma-induced polymerization and metal evaporation techniques [12]. The chemical methods mainly include the reduction of metal inside the polymer i.e. the intermatrix synthesis of these composites [13, 14].

Mesoporous ion exchange resins were employed to prepare polystyrene $\gamma$-$Fe_2O_3$ nanocomposites with magnetic functionality [15, 16]. The size of the magnetic oxide can be predetermined depending on the choice of the particular resin which is again graded according to the channels in the porous resin. Thus, a judicious choice of the polymer matrix determines the size of the oxide particle. This study caught the imagination of many researchers and various metal oxide polymer nanocomposites were prepared [17–19]. The availability of various ion exchange resins commercially were an added attraction to these researchers. However, for the fabrication of metal–polymer composites, a different route has to be adopted. For example, mesoporous ion exchange resins can be a template matrix where suitable metal ions are anchored to the functional resins followed by their subsequent reduction inside the polymer network. This method is generally known as the ion exchange reduction process.

Nickel nanoparticles embedded in a polymer matrix are important not only from a commercial point of view but also from a fundamental perspective. They are ideal templates for studying the size effects on the magnetic properties. The optical properties of these particles at the nanolevel also assume significance. The interaction between metal nanoparticles embedded in a polymer matrix can also be an interesting topic of investigation. The method of ion exchange has been employed for the incorporation of metal oxide nanoparticles in the host matrix [15, 16]. However, reports employing the method of ion exchange resins for the preparation of passivated magnetic metal particles are not very common.

Nickel polymer nanocomposites can be synthesized by the method of reduction using two different templates namely, strongly acidic cation exchange resin and weakly acidic cation exchange resins. Since both the strong and weak resins are characterized by their channels and pores, respectively, the overall properties of the composite need not be identical vis a vis the nature of the embedded nano nickel inside the matrix, the impurity phase, etc. This investigation is an attempt to synthesize nickel nanocomposites using two different matrices having different functional groups and different structures and to study their structural and magnetic properties with a view to optimize the method of synthesis by cycling to increase the net magnetization of the nanocomposite. The exact determination of the amount of nickel on the composite is also important. Therefore, compositional analysis using techniques like Inductively Coupled Plasma Analysis (ICP)/ Energy Dispersive X-ray Spectrum Analysis (EDS) enables one to determine the exact composition of nickel in the synthesized nanocomposites. The morphological and structural aspects are investigated using X-Ray diffraction, Transmission Electron Microscopy, and Scanning Electron Microscopy. The effect of cycling on the magnetic properties of these composites form another objective. Hence, a complete study on the nanocomposites is undertaken in the present investigation. The motivation of the present study is not only to synthesize self protected nickel nanoparticles in a porous network having two structures, but also to investigate how the structural and magnetic properties differ in these two matrices. The different type of interactions between metal nanoparticles trapped in a dense matrix and porous matrix can be quite interesting.

## Experimental

### Synthesis of Metal Polystyrene Nanocomposite

The ion exchange resins in the form of beads are basically functionalized polystyrene which are cross linked with divinyl benzene having a three dimensional porous polymer matrix. Ion exchange resins have been classified based on the charge on the exchangeable counterion (cation exchanger or anion exchanger) and the ionic strength of the bound ion (weak and strong). Ion exchange resins are manufactured in two physical structures, gel or microporous (http://www.sigmaaldrich.com/aldrich/brochure/al_pp_ionx.pdf). Gel type resins are homogenous, have no discrete pores, the channels act as pores while macroporous resins are referred to as fixed pore resins. The strongly acidic resins (gel type) are functionalized with sulfonic acid group while the weakly acidic resins (macroporous) are functionalized using carboxylic acid groups (Fig. 1a, b). Both these resins are 8%

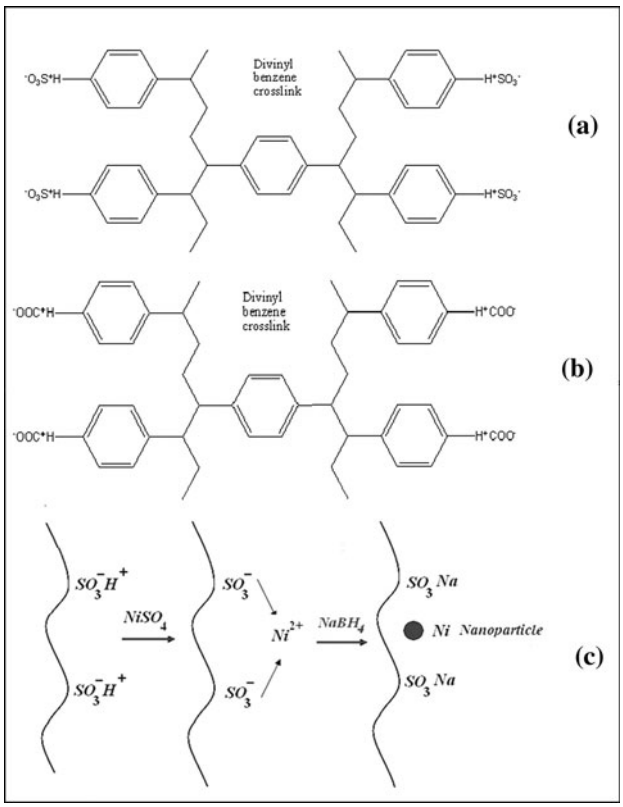


**Fig. 1** **a** Strongly acidic cation exchange resin (SAC). **b** Weakly acidic cation exchange resin (WAC) and **c** Schematic of synthesis of Nickel–polystyrene composites

cross-linked polymer of polystyrene and divinyl benzene, which have exchangeable $H^+$ ions associated with their respective functional groups.

The presence of functional groups in the polymer matrix permits us to load them with metal cations by using conventional ion exchange mechanism. For the preparation of nickel polystyrene nanocomposites, SRC-120 (Amberlite IRC-120) and WRC-50 (Amberlite IRC-150) are initially soaked separately for 24 h in distilled water so that they are swollen. A saturated solution of 1 M $NiSO_4$ (Merck) is filled in a reaction column along with soaked resin for about 24 h. The ion exchange process is initiated at this stage. The $Ni^{2+}$ ions are exchanged with the $H^+$ ions in the resin. Further reduction of $Ni^{2+}$ ions to Ni inside the polymer matrix occur with the addition of $NaBH_4$. Dilute solution of $NaBH_4$ is added drop wise to the resin. Nickel ions are reduced to metallic nickel particles by the following reaction:

$$2Ni^{2+} + 4BH^{4-} + 9H_2O \rightarrow Ni_2B + 12H_2 + 3B(OH)_3, \quad (1)$$

$$4Ni_2B + 3O_2 \rightarrow 8Ni + 2B_2O_3. \quad (2)$$

The resins are then washed several times with distilled water to remove the by-products of the reaction. Thus, nanosized Ni particles are expected to be trapped within the interstitial channels of polymer beads. The schematic of the synthesis is depicted in Fig. 1c. A similar procedure using WAC is adopted for the incorporation of nickel nanoparticles inside the matrix except that $SO^{3-}$ $H^+$ is replaced by COO–$H^+$ in WAC. The metal-loading reduction cycle can be repeated to increase the metal content in the composites. Hence, an increased loading is achieved by cycling the samples. The samples are cycled several times and are labeled as SAC0 to SAC16 and WAC2 to WAC10. The physical appearance of the pure ion exchange resin and that of Nickel polymer composites are depicted in Fig. 2a, b.

## Characterization

X-Ray diffraction patterns of the samples were recorded using an X-Ray Powder Diffractometer (Rigaku Dmax—C) using Cu-K$\alpha$ radiation ($\lambda = 1.5405$ Å). The diffraction patterns were taken in the range from $2\theta = 35°$ to 110°. Lattice parameter was calculated assuming cubic symmetry. The average crystallite size was estimated by using Debye Scherer's formula. The particle size was also determined by subjecting the samples to Transmission electron microscopy (Joel JEM-2200 FS). Energy Dispersive X-ray Spectra (EDS) was also obtained. Thermo Electron Corporation, IRIS INTRPID II XSP model ICP was used for elemental analysis. Magnetic measurements were performed using a vibrating sample magnetometer (model EG & G PAR 4500) under an applied magnetic field of 15kOe. High resolution Scanning Electron Microscopy was employed to check the morphology of the samples (JSM-6335 FESEM).

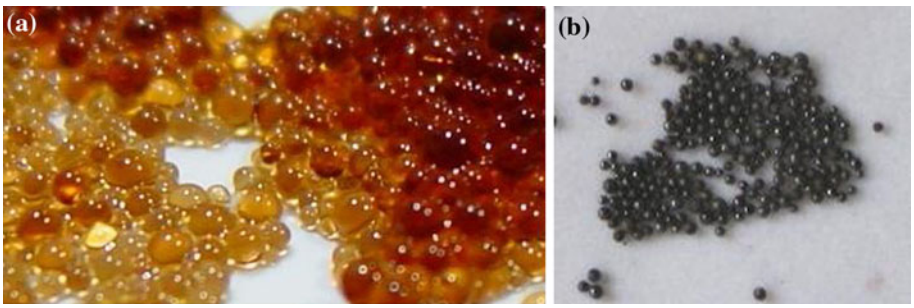


**Fig. 2** **a** Photographs of Polystyrene beads (SAC) and **(b)** Nickel–Polystyrene nano composites (SAC 12)

## Result and Discussion

### Structural Characterization

The X-ray diffraction patterns of the SAC and WAC nanocomposites are shown in Figs. 3 and 4. The patterns are characteristic of an fcc lattice consisting of nickel nanoparticles without any detectable traces of any impurity. No peaks corresponding to Nickel oxide were observed in the case of samples on SAC. However, in the case of samples on WAC, the XRD pattern consists of characteristic peaks of Nickel and Nickel oxide. The appearance of a kink in the main at 44° indicate the presence two phases, one that of Nickel (44.5°—(111)) and the other corresponding to Nickel oxide (43.3°—(200) plane) in the composite. The two peaks almost overlap and hence the difficulty in distinguishing one from the other. Due to the macroporous nature of WAC, compared to the gel type nature of SAC, the chances of formation of oxide is more in the case of WAC than SAC. The lattice parameter '*a*' and crystallite size calculated using Debye Scherer formula. In SAC, the particle size is found to be ~13 nm. The lattice parameter values are found to be 3.522 Å for SAC and 3.561 Å for WAC. The lattice parameter of bulk nickel is 3.523 Å (JCPDS 04-1027) and of Nickel oxide is 4.117 Å (JCPDS 02-7440). The widening of the lattice in WAC Ni can be attributed to the interfacial stress that originates from the lattice mismatch between Nickel and Nickel Oxide [20, 21].

The effect of cycling on the structural parameters of nickel composites is depicted in Figs. 5 and 6. The XRD of samples indicates that the formation of crystalline nickel particles occurs after 2 cycles of reduction. With cycling,

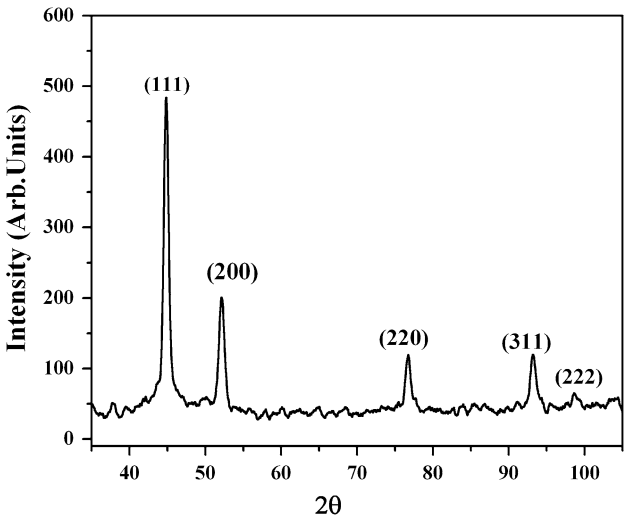


**Fig. 3** XRD pattern of Nickel Polymer composite (SAC-16)

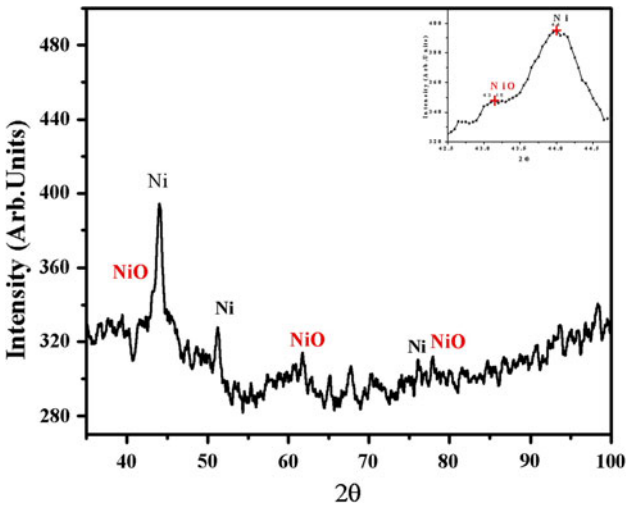


**Fig. 4** XRD pattern of Nickel Polymer composite (WAC-10) (*inset enlarged view*)

the crystallinity of the sample is found to be increasing due to the addition of more and more nickel nanoparticles after each metal loading reduction cycle. The variation in intensity of the peaks reveals the increased number of crystalline paricles in the matrix (Fig. 5). The average crystallite size for all the cycled (from SAC4–SAC16) samples is found around 13 nm.

Although there is an increase in the crystalline behavior of the composites (SAC), the particle size of the nanoparticles incorporated in the matrix do not undergo any change with cycling. Hence, it is to be presumed that the nickel nanoparticles are trapped in the polymer matrix as soon as they are formed and further growth of nanoparticles is inhibited. After each cycle, it is the concentration of nickel nanoparticles in the matrix which is increasing. The improved crystallinity of the composites is manifested in the XRD pattern. The absence of any oxide phase in all the cycled samples of SAC confirms the formation of self protected metal nanoparticles. On the other hand, the presence of Nickel oxide in WAC composites points toward the existence of nickel oxide layer on the nickel particles.

From ICP measurements, the nickel content in the composite is calculated and the percentage of nickel in the composite is found to be increasing with cycling and is shown in Fig. 7. For SAC16, the maximum loading of 21% is obtained which is consistent with our earlier studies on polystyrene nanocomposites [19]. For the maximum cycled WAC resin, 16% of Nickel by weight was obtained.

The scanning electron micrographs of SAC-12 and WAC-8 are shown in Fig. 8a, b. The dense channeled structure of SAC is quite evident from the micrograph while the porous character of WAC is apparent from the

**Table 1** Magnetic parameters of SAC–Ni and WAC–Ni nanocomposites

| | $M_s$ (emu/g) (300 K) | $M_s$ (emu/g) (100 K) | $H_c$ (Oe) (300 K) | $H_c$ (Oe) (100 K) | $T_c$ K |
|---|---|---|---|---|---|
| SAC-16 | 7.6 | 10 | 80 | 120 | 707 |
| WAC-8 | 2.06 | 3.03 | 35 | 90 | 689 |

$M_s$ saturation magnetization, $H_c$ coercivity, $T_c$ Curie temperature

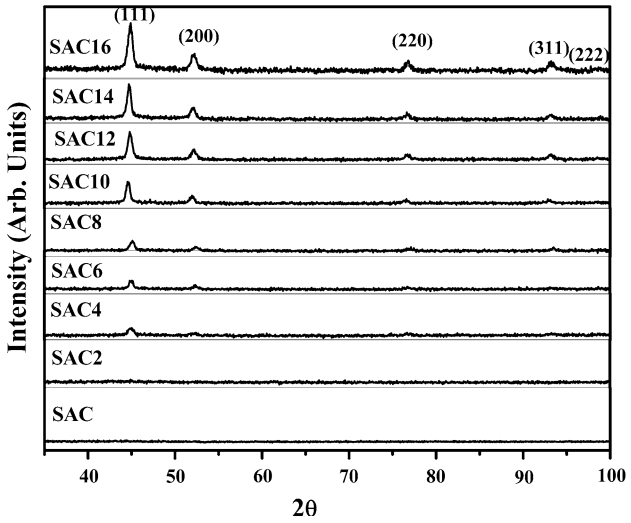


**Fig. 5** The XRD patterns of the composites from SAC to SAC16

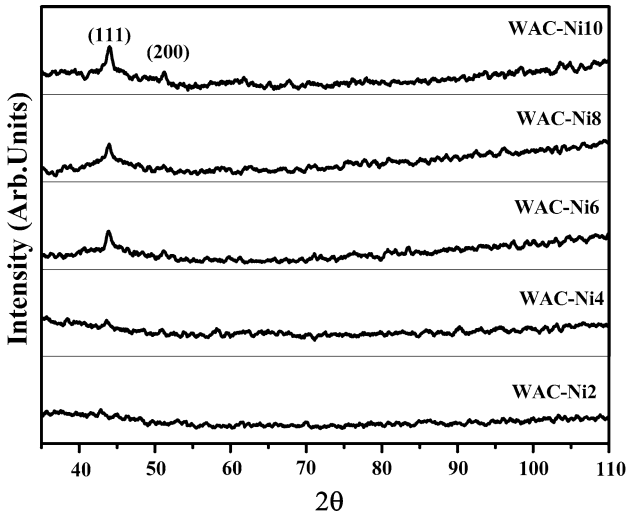


**Fig. 6** The XRD patterns of the composites from WAC 2 to WAC10

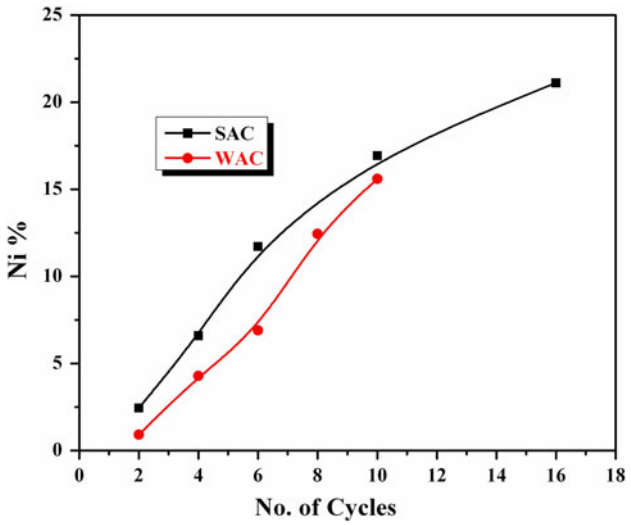


**Fig. 7** Nickel content in SAC and WAC composites

images. Some of the anchored nickel nanoparticles in the channels can be noticed in SAC-12.

Representative TEM micrographs of samples are shown in Fig. 9a, b. The particle size is estimated to be 19 nm for the Nickel in SAC composite. Discrete pores of the WAC resins with sizes in the range 60–70 nm along with embedded nickel nanoparticles are clearly seen in the TEM. However, the nanoparticles are found to have larger size (around 40 nm) in the weak resin. This may be due to the agglomeration of the nanoparticles within the pore. EDS patterns of the composites confirm the presence of nickel in the polystyrene matrix (Fig. 10a, b).

## Magnetic Characterization

Room temperature hysteresis curves of the two composites are shown in Figs. 11 and 12. The hysteresis loop parameters evaluated from the hysteresis curves are given in Table 1. The hysteresis curves of SAC composites are typical of ferromagnetic nanoparticles. The nature of the M–H curve in WAC is indicative of the presence of an antiferromagnetic component. The antiferromagnetic nature of the Nickel oxide layer in the WAC composite may be contributing to this features. Therefore, the WAC composites may contain nickel–nickel oxide core–shell nanostructures. An exchange bias coupling can occur between the two phases [22]. The non saturating nature of magnetization curves of WAC composites supports this argument.

The composites are showing saturation property at the 2nd cycle itself. This makes clear the formation of pure nickel nanoparticles in the resins. With cycling, the saturation magnetization values are showing an increasing trend. It is the increase in metal loading after each cycling

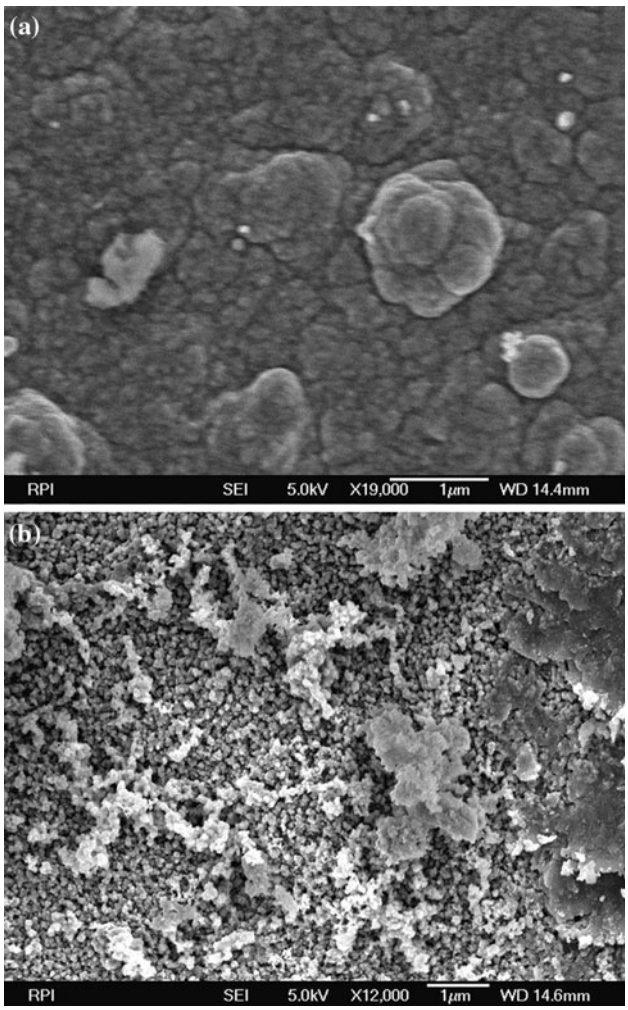


**Fig. 8** **a** SEM images of SAC-12 and **b** WAC-8 nanocomposites

that resulted in the increased $M_s$ values. The increase in $M_s$ is found to be slow at higher cycles in both the composites. The coercivity values of the composites are found to be around 100 Oe. The coercivity values show a little variation after the second cycle in SAC composites while a clear variation is observed in WAC composite (insets of Figs. 11, 12). Accordingly, the formation of self-protected elementary nanoparticles of nickel can be assured in the samples on SAC. In the case of WAC composites, the formation of an oxide layer over the nanoparticles is expected.

In both the composites, the cycling enhances the magnetization values. The magnetization value of the composite is entirely due to the magnetic nickel nanoparticles in the matrix. The $M_s$ in bulk nickel is 55 emu/g and the effective $M_s$ values of the nickel nanoparticles embedded in the matrix can be estimated from the percentage of Nickel content estimated from ICP analysis of these composites. It can be seen that the maximum cycled sample has an effective magnetization ($M_s$ at 100 K/Nickel content) of 47.39 emu/g for SAC-16 and 24.44 emu/g for WAC-8. The decrease in $M_s$ compared with the bulk might be due to the decrease in particle size and the accompanied increase in surface area. The presence of nickel oxide along with nickel also could be a contributing factor for the enhanced reduction of nickel nanoparticles embedded in the WAC-resin [20]. Reduction in $M_s$ in Ni nanoparticles also could be due to the presence of amorphous nickel and the non magnetic or weakly magnetic interfaces [23].

The temperature dependence of magnetization ($M$ vs. $T$) for the two composites is depicted in Figs. 13 and 14. The Curie temperature ($T_c$) was estimated by derivative graphs ($dM/dT$ graph—given as insets in Figs. 13, 14) of $M$–$T$ curves for the composites. The $T_c$ values of the nanoparticles were found to be larger than that observed for their bulk counterparts. The estimated $T_c$ values were around 707 and 689 K for the SAC and WAC composites, respectively. It is to be noted that $T_c$ values for bulk Nickel is 631 K. It is predicted that the curie temperature of nanoparticles depends on both the size and shape [24]. For systems of embedded nanoparticles, Curie temperature also depends on the interaction between the particles in the matrix. It has been reported that there exists different degrees of spin–spin interaction between inner and surface atoms in the nanoparticles [25, 26]. These interaction could

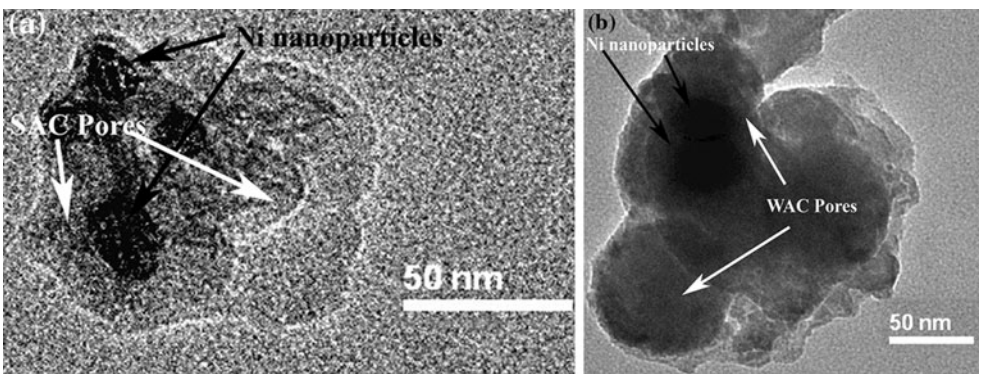


**Fig. 9** **a** TEM images of SAC-16 and **b** WAC-8 nanocomposites

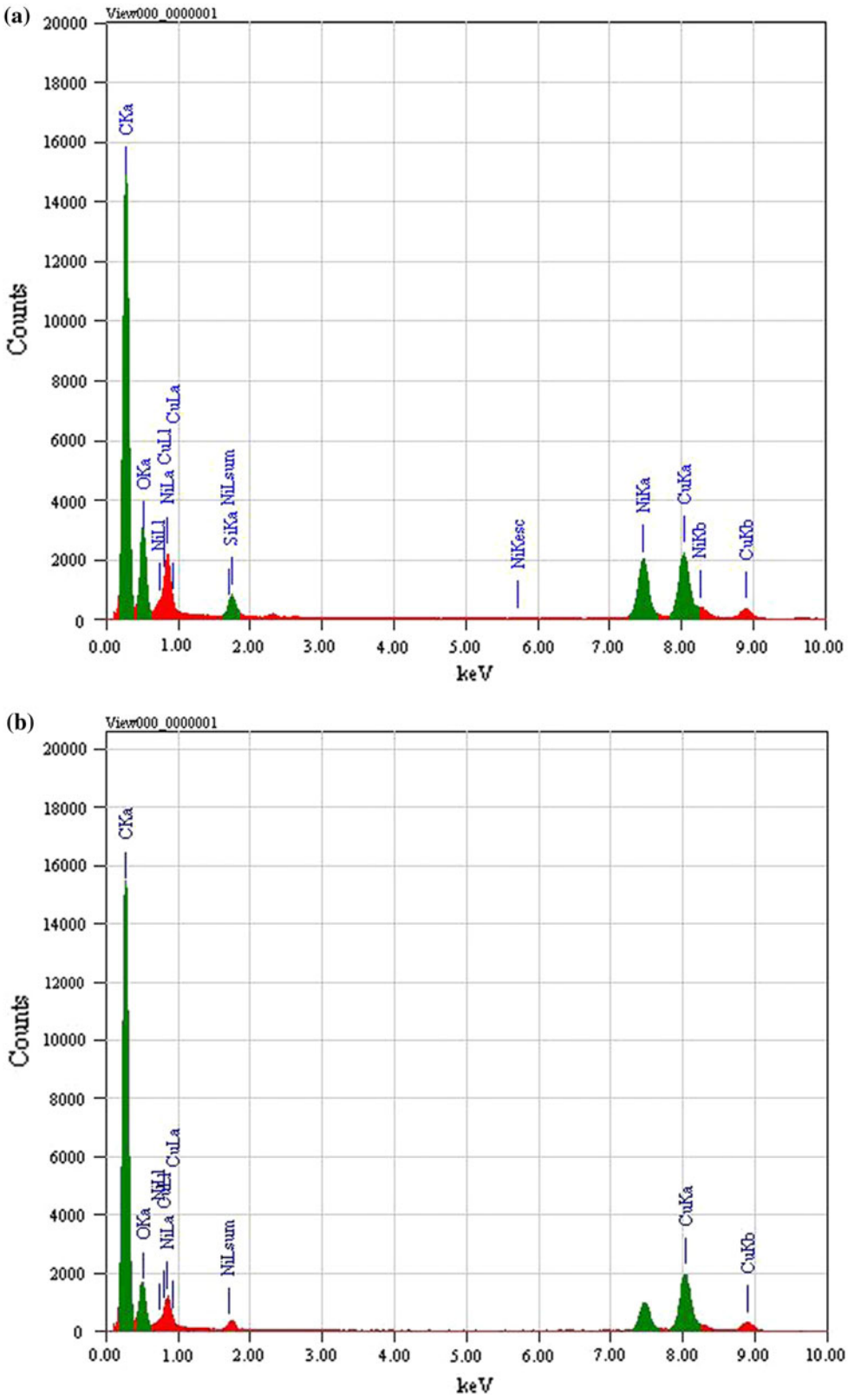


**Fig. 10** **a** EDS patterns of SAC-16 and **b** WAC-8 nanocomposites

contribute to the enhancement of $T_c$ in nanocomposites. The magnetic transition in the WAC composites around 560 K points toward the antiferromagnetic transition of nickel oxide [27]. Accordingly, the SAC metal composites were found to have superior magnetic characteristics compared to the WAC composites.

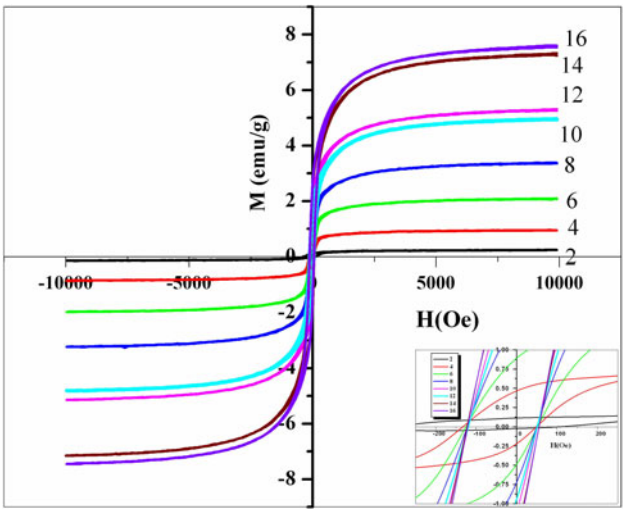


**Fig. 11** Room temperature magnetization curves for the SAC nanocomposites (*inset gives enlarged view*)

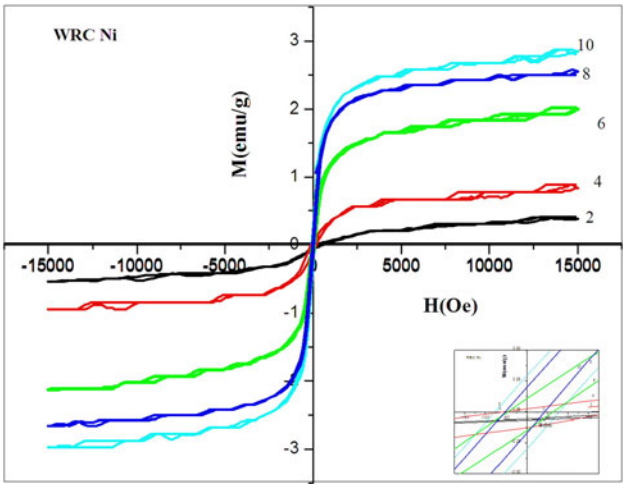


**Fig. 12** Room temperature magnetization curves for the WAC nanocomposites (*inset gives enlarged view*)

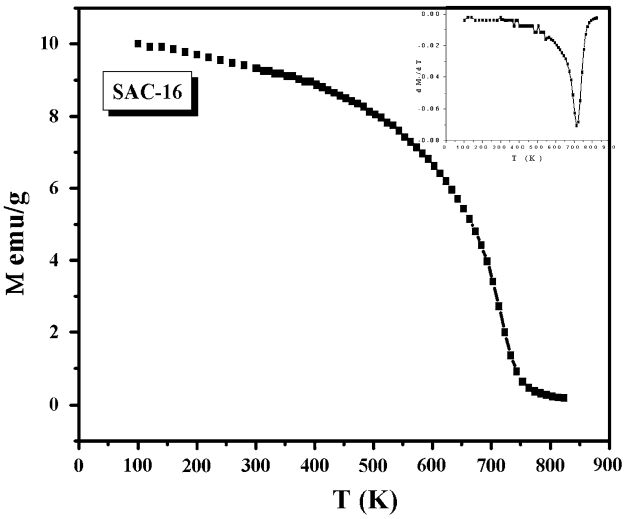


**Fig. 13** *M–T* curve for SAC-16 (d*M*/d*T* vs. *T* graph in the *inset*)

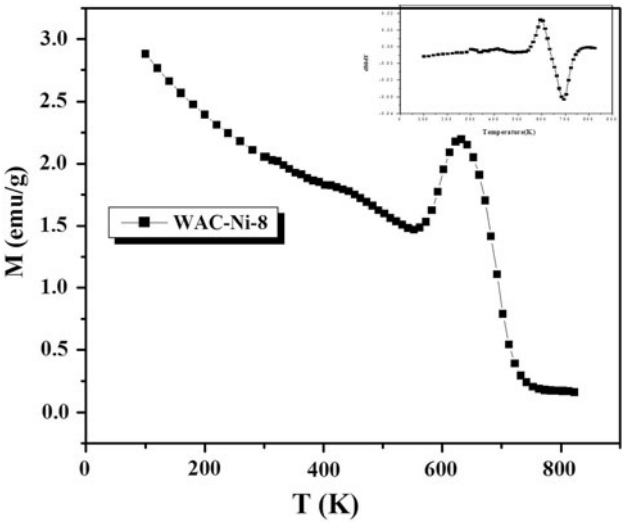


**Fig. 14** M–T curve for WAC-10 (d*M*/d*T* vs. *T* graph in the *inset*)

## Conclusions

Nickel–polystyrene nanocomposites are synthesized by the intermatrix ion exchange synthesis where we have used strongly acidic cationic Exchange Resin (SAC) and weakly acidic cationic Exchange Resin (WAC) with cationic exchange sites as the parent matrices. The sequential loading of the cationic exchange sites with metal ions and their subsequent reduction using Sodium borohydride resulted in Ni–Polystyrene nanocomposites. The crystallinity and magnetic characteristics are modified by repeating the loading reduction cycle. The effect of cycling on the structural and magnetic properties of the composites is also investigated. The XRD patterns of the cycled samples confirmed that the there is no particle growth with cycling. These investigations indicate that SAC composites contain phase pure nickel nanoparticles trapped in the interstitial channels of the polystyrene matrix and their further growth is inhibited. On the other hand, WAC composites contain two distinct phases of Nickel and Nickel oxide. Comparison of the structural and magnetic properties of the two types of composites showed that the SAC resin composites are better in structural as well as magnetic properties compared to WAC resin composites. These interesting attributes of the magnetic nanocomposites can be tailored for promising applications. Moreover, optical and electrical characterization of these composites can be promising areas of research for device applications.

**Acknowledgments** EVG acknowledges Cochin University of Science and Technology for the Research Fellowship and STIC, CUSAT

for the ICP measurements. KAM thanks University Grant Commission, Government of India for the financial assistance received under UGC minor project. GS acknowledges Department of Collegiate Education, Govt. of Kerala. Al–Omari would like to thank the Sultan Qaboos University for the support under Grant number IG-SCI-PHYS-09-01. MRA acknowledges Kerala State Council for Science, Technology and Environment (C.O. No. (T)/159/SRS/2004/CSTE dated: 25-09-2004), Kerala, India, for the financial assistance.



## References

1. H. Gleiter, Prog. Mater. Sci. **33**, 223 (1990)
2. K.J. Klabunde, C. Mohs, in *Chemistry of Advanced Materials: An Overview*, ed. by L.V. Interrante, M.J. Hampden-Smith (Wiley-VCH, New York, 1998), p. 271
3. M.M. Miller, G.A. Prinz, S.F. Cheng, S. Bounnak, Appl. Phys. Lett **81**, 2211 (2002)
4. G. Torok, V.T. Lebedev, L. Cser, G. Kali, M. Zrinyi, Physica B **297**, 40 (2001)
5. Y. Lu, X. Lu, B.T. Mayers, T. Herricks, Y. Xia, J. Solid State Chem. **181**, 1530 (2008)
6. D.K. Lee, Y.H. Kim, X.-L. Zhang, Y.S. Kang, Curr. Appl. Phys. **6**, 786 (2006)
7. A.D. Pomogailo, G.I. Dzhardimalieva, A.S. Rozenberg, D. Muraviev, J. Nanoparticles Res. **5**, 497 (2003)
8. O. Santini, D.H. Mosca, W.H. Schreiner, R. Marangoni, J.L. Guimaraes, F.A. Wypych, J.A. Oliveira, J. Phys. D Appl. Phys. **36**, 428 (2002)
9. E.R. Leite, N.L.V. Carreño, E. Longo, A. Valentini, L.F.D. Probst, J. Nanosci. Nanotechnol. **2**, 89 (2002)
10. Z.P. Huang, D.Z. Wang, J.G. Wen, M. Sennett, H. Gibson, Z.F. Ren, Appl. Phys. A **74**, 387 (2002)
11. L. Levy, Y. Sahoo, K.S. Kim, E. Bergey, P.N. Prasad, Chem. Mater. **14**, 3715 (2002)
12. G. Kickelbick, Prog. Polym. Sci. **28**, 83 (2003)
13. D.N. Muraviev, Chem Scripta **29**, 9 (1989)
14. R. Brayner, M.-J. Vaulay, F. Fie′vet, T. Coradin, Chem. Mater. **19**, 1190 (2007)
15. R.F. Ziolo, E.P. Giannelis, B.A. Weinstein, M.P. O'Horo, B.N. Ganguly, V. Mehrotra, M.W. Russell, D.R. Huffman, Science **257**, 219 (1992)
16. R.D. Shull, L.H. Bennett, Nanostruct. Mater. **1**, 83 (1992)
17. M.L. Wang, C.H. Wang, W. Wang, Mater. Chem. Phys. **104**, 162 (2007)
18. K.A. Malini, M.R. Anantharaman, S. Sindhu, C.N. Chinnasamy, N. Ponpandian, A. Narayanasamy, B. Balachandran, V.N. Shivasankarapillai, J. Mater. Sci. **36**, 821 (2001)
19. S. Swapna Nair, M. Mathews, P.A. Joy, S.D. Kulkarni, M.R. Anantharaman, J. Magn. Magn. Mater. **283**, 344 (2004)
20. B. Rellinghaus, S. Stappert, E.F. Wassermann, H. Sauer, B. Spliethoff, Eur. Phys. J. D. **16**, 249 (2001)
21. H. Hofmeister, F. Huisken, B. Kohn, Eur. Phys. J. D. **9**, 137 (1999)
22. T. Seto, H. Akinaga, F. Takano, K. Koga, T. Orii, M. Hirasawa, J. Phys. Chem. B **109**, 13403 (2005)
23. I. Turek, J. Hafner, Phys. Rev. B **46**, 247 (1992)
24. R. Evans, U. Nowak, F. Dorfbauer, T. Shrefl, O. Mryasov, R.W. Chantrell, G.J. Grochola, Appl. Phys. **99**, 08G703 (2006)
25. D.H. Cole, K.R. Shull, L.E. Rehi, Saucer, P. Baldo, Phys. Rev. Lett. **78** 5006, (1997)
26. X.Y. Lang, W.T. Zhang, Q. Jiang, Phys. Rev. B **73**, 2244 (2006)
27. D.J. Craik, *Magnetic Oxides*, Part 1 (Wiley, New York, 1997)